Volume 58(5): 429–441, 2010
Journal of Histochemistry & Cytochemistry
http://www.jhc.org

ARTICLE

Quantitative and Qualitative Alterations of Heparan Sulfate in Fibrogenic Liver Diseases and Hepatocellular Cancer

Péter Tátrai, Krisztina Egedi, Áron Somorácz, Toin H. van Kuppevelt, Gerdy ten Dam, Malcolm Lyon, Jon A. Deakin, András Kiss, Zsuzsa Schaff, and Ilona Kovalszky

Second Department of Pathology (PT,ÁS,AK,ZS) and First Department of Pathology and Experimental Cancer Research (PT,KE,ÁS,IK), Semmelweis University, Budapest, Hungary; Nijmegen Center for Molecular Life Sciences, Radboud University Nijmegen Medical Center, Nijmegen, The Netherlands (THvK,GtD); and Cancer Research UK Glyco-Oncology Group, School of Cancer and Imaging Sciences, Paterson Institute for Cancer Research, University of Manchester, Manchester, United Kingdom (ML,JAD)

SUMMARY Heparan sulfate (HS), due to its ability to interact with a multitude of HS-binding factors, is involved in a variety of physiological and pathological processes. Remarkably diverse fine structure of HS, shaped by non-exhaustive enzymatic modifications, influences the interaction of HS with its partners. Here we characterized the HS profile of normal human and rat liver, as well as alterations of HS related to liver fibrogenesis and carcinogenesis, by using sulfation-specific antibodies. The HS immunopattern was compared with the immunolocalization of selected HS proteoglycans. HS samples from normal liver and hepatocellular carcinoma (HCC) were subjected to disaccharide analysis. Expression changes of nine HS-modifying enzymes in human fibrogenic diseases and HCC were measured by quantitative RT-PCR. Increased abundance and altered immunolocalization of HS was paralleled by elevated mRNA levels of HS-modifying enzymes in the diseased liver. The strong immunoreactivity of the normal liver for 3-*O*-sulfated epitope further increased with disease, along with upregulation of 3-OST-1. Modest 6-*O*-undersulfation of HCC HS is probably explained by Sulf overexpression. Our results may prompt further investigation of the role of highly 3-*O*-sulfated and partially 6-*O*-desulfated HS in pathological processes such as hepatitis virus entry and aberrant growth factor signaling in fibrogenic liver diseases and HCC.
(J Histochem Cytochem 58:429–441, 2010)

KEY WORDS
heparan sulfate
liver cirrhosis
hepatocellular carcinoma

HEPARAN SULFATE (HS) chains, the highly sulfated glycosaminoglycans (GAGs) attached to the protein core of heparan sulfate proteoglycans (HSPGs), are intricately involved in a variety of physiological processes such as morphogenesis, wound healing, regulation of cell differentiation and growth, and establishment of cell–cell and cell–extracellular matrix contacts (Bishop et al. 2007). HSPGs can also show their dark face in diseases: they may promote tumor growth, invasion, and angiogenesis (Blackhall et al. 2001; Fuster and Esko 2005; Fears and Woods 2006; Iozzo et al. 2009). HS owes most of its importance to its dynamic interactions with a multitude of HS-binding factors. In particular, its complex formation with growth factors and their receptors is indispensable for proper receptor activation and signaling (for example, see Harmer 2006). Also, HS acts as a coreceptor for the cellular entry of viruses including herpes simplex virus 1 (Shukla et al. 1999), hepatitis B and C viruses (Barth et al. 2003; Schulze et al. 2007), and many others. Interactions between HS and its ligands are fine-tuned by the sulfation pattern of HS (Ashikari-Hada et al. 2004), as well as the

Correspondence to: Péter Tátrai, PhD, Second Department of Pathology, Semmelweis University, 93 Üllői út H-1091 Budapest, Hungary. E-mail: peter.tatrai@biomembrane.hu

Received for publication September 27, 2009; accepted January 12, 2010 [DOI: 10.1369/jhc.2010.955161].

enzyme heparanase (HPSE), which mobilizes bound ligands by specifically cleaving HS chains (Vlodavsky et al. 2007).

Not only does each organ and tissue have its own well-defined HS profile (Dennissen et al. 2002), but HS undergoes characteristic qualitative and quantitative alterations under pathological conditions. Differences between healthy organs, as well as those between the healthy and diseased states of the same organ, are attributable to differential expression of the various HSPGs on one hand and to altered regulation of the enzymatic machinery of HS synthesis and modification on the other. Pathologic changes of HSPG composition, as well as of HS synthesis and structure, have been described in non-malignant conditions such as central nervous system injury (Properzi et al. 2008) and chronic kidney disease (Lauer et al. 2007; Rops et al. 2007) and also in malignant tumors such as pancreatic ductal cancer (Korc 2007).

Although the expression and tissue distribution of HSPGs in healthy and diseased liver have been investigated (Roskams et al. 1995,1996,1998; Kovalszky et al. 1998), little is known about the abundance and localization of various HS structural motifs in the adult human liver and the changes that HS chains and their processing enzymes undergo in chronic liver diseases. In our earlier work, we demonstrated that HS from hepatocellular carcinoma (HCC) and its peritumoral tissue possesses altered biological properties compared with normal liver HS (Dudás et al. 2000), but the structural basis for this difference remained to be defined. The disaccharide composition of HS from human liver has been characterized (Vongchan et al. 2005), but neither tissue distribution nor pathologic alterations have been studied. Expression of the *N*-deacetylase/*N*-sulfotransferases NDST-1 and NDST-2 and of the *O*-sulfotransferases 3-OST-1, 3-OST-3A, 3-OST-3B, and 6-OST-1 have been detected in human liver (Shworak et al. 1999; Ledin et al. 2006); however, the possible implication of these or other sulfotransferases in liver pathogenesis has not been explored. Most data for HS-modifying enzymes with relevance to liver disease have been gathered regarding HPSE and the 6-*O*-endosulfatases Sulf1 and Sulf2. While upregulation of HPSE and Sulf2 appear to promote the progression of HCC, Sulf1 is instead believed to act as a suppressor of HCC growth (Xiao et al. 2003; Lai et al. 2008b).

In the present work, we set out to characterize the HS profile of normal human liver, as well as alterations in the HS immunopattern related to liver fibrogenesis and carcinogenesis, using sulfation-specific antibodies. As we had access to a well-established rodent model of liver fibrogenesis and hepatocarcinogenesis, we were able to compare the HS immunopatterns of the healthy and diseased rat liver with human counterparts. Changes in the amount and distribution of HS were interpreted in the context of altered expression of four major liver HSPGs: syndecan-1, perlecan, agrin, and glypican-3 (Roskams et al. 1995; Zhu et al. 2001; Tátrai et al. 2006). HS samples from normal liver and HCC were also compared by using disaccharide analysis. Additionally, we measured mRNA expression levels of nine HS-modifying enzymes formerly reported to be expressed in the liver (HPSE, NDST-1 and -2, 2-OST-1, 3-OST-1 and -3B, 6-OST-1, and Sulf1 and Sulf2) across normal, fibrogenic, and HCC tissues to look for possible links between structural alterations of HS and disease-associated changes in gene expression.

Materials and Methods

Patient Material

Human experimental material was obtained from the Transplantation and Surgical Clinic, the First Department of Surgery, and the Department of Forensic Medicine of the Semmelweis University, Budapest, Hungary. Formalin-fixed, paraffin-embedded tissues (one peritumoral tissue from a hepatic adenoma patient, and two tissue blocks from an HCC patient with cirrhosis) were obtained from the archive of the Second Department of Pathology, Semmelweis University. Fresh liver samples were taken from 21 HCC and 3 focal nodular hyperplasia (FNH) patients, as well as from 8 healthy individuals who died in accidents. Peritumoral tissue was available from 15 HCC patients (4 patients with cirrhosis, 4 patients with fibrosis, and 7 patients without fibrosis) and from 1 FNH patient (without fibrosis). Specimens were snap-frozen, stored in liquid nitrogen or at −80C and subsequently used for immunofluorescence studies, as well as for the isolation of GAGs and total RNA. Patients, or their legal representatives, gave written informed consent to the experimental use of such tissues. Studies were carried out with permission from the ethical committees of the respective Institutions.

Animal Experimental Material

Four male Wistar rats obtained from Charles River (Sulzfeld, Germany) were subjected to a fibrogenic/hepatocarcinogenic regimen consisting of a single-dose administration of diethylnitrosamine and a 6-week combined phenobarbital and carbon tetrachloride (DPC) treatment. The details of the protocol were described previously by Zalatnai and Lapis (1994). All animals, when killed at week 16, had histologically proven cirrhosis and multifocal HCC. Animals received humane care in compliance with guidelines of the institution and the National Institutes of Health.

Immunofluorescence

Tissue samples from human non-fibrotic liver (n=2), FNH patients (n=2), cirrhosis patients (n=3), and HCC patients (n=5), as well as from the liver of

1 normal and 4 DPC-treated rats were subjected to immunofluorescence analysis using the phage display-derived, sulfation-specific, single-chain anti-HS antibodies AO4B08, EV3C3, HS4C3, HS4E4, and RB4Ea12. The non-HS-reactive MBP49 antibody was included as a negative control (results not shown). Epitope specificities of the antibodies used are shown in Table 1. Furthermore, rabbit polyclonal anti-human syndecan-1 (BioVision; Mountain View, CA) and mouse monoclonal anti-human perlecan, clone 7B5 (Invitrogen; Carlsbad, CA) were used for double-fluorescence labeling of human tissues (one non-fibrotic peritumoral sample, two cirrhosis samples, and five HCC samples). In the case of syndecan-1 and perlecan, primary antibodies were replaced by the appropriate non-immune sera for negative control slides (results not shown).

Sections of 10 μ were cut from the frozen liver specimens, fixed in cold methanol for 20 min and in cold acetone for 10 sec, and blocked with 5% BSA in PBS. Phage display antibodies containing a vesicular stomatitis virus glycoprotein (VSV-G) tag were applied to the slides in a dilution of 1:2 overnight at 4C. Subsequently, slides were incubated with a 1:100 dilution of mouse anti-VSV-G antibody clone P5D4 (Sigma-Aldrich; St. Louis, MO) and finally with a 1:200 dilution of Alexa Fluor 488-conjugated anti-mouse antibodies (Invitrogen). Syndecan-1 and perlecan antibodies were diluted 1:100 and detected with the appropriate Alexa Fluor 488- and 568-conjugated secondary antibodies (Invitrogen). Nuclei were stained with 4′,6-diamidino-2-phenylindole.

Table 1 HS epitopes recognized by phage display-derived antibodies

Antibody	Modifications involved in binding
HS4C3[a]	*N*-sulfation (essential)[d]
	6-*O*-sulfation (essential)[d]
	3-*O*-sulfation (essential)[d]
	2-*O*-sulfation[d]
HS4E4[b,c]	*N*-sulfation
	N-acetylation
	Iduronate
	Unspecified *O*-sulfated epitopes required?
	High 2- and 6-*O*-sulfation reduce binding
AO4B08[b]	*N*-sulfation
	Iduronate
	Internal 2-*O*-sulfation[e]
	High 6-*O*-sulfation[e]
RB4Ea12[c]	*N*-acetylation
	N-sulfation
	6-*O*-sulfation
EV3C3[c]	Unknown
MPB49[c]	Not reactive with HS

[a]Data from ten Dam et al. (2006).
[b]Data from Kurup et al. (2007).
[c]Data from Wijnhoven et al. (2008).
[d]Antibody HS4C3 was shown to recognize the antithrombin-binding minimal pentasaccharide GlcNAc/S–GlcA–GlcNAc/NS3,6diS–IdoA2S–GlcNS,6S, as well as other 3-*O*-sulfated motifs.
[e]Antibody AO4B08 requires an internal 2-*O*-sulfated iduronic acid residue and more than one 6-*O*-sulfate within a target octasaccharide.
Epitopes are not sequentially defined but involve the presence of various structural features in the target oligosaccharide, while other features may be inhibitory to reactivity. HS, heparan sulfate.

Immunohistochemistry

Serial sections (3 μ thick) of formalin-fixed, paraffin-embedded human tissues (sampled from peritumoral non-fibrotic liver of a hepatic adenoma patient, a cirrhotic liver, and HCC) were subjected to immunohistochemistry for detection of agrin and glypican-3. Steps were performed at room temperature (24C) unless otherwise noted. For the immunodetection of agrin, sections were deparaffinized and rehydrated, immersed in boiling Target Retrieval Solution (Dako; Glostrup, Denmark) in a pressure cooker for 5 min, digested with 0.5 mg/ml Pronase E (Sigma-Aldrich) for 5 min, treated with 10% hydrogen peroxide in methanol for 15 min to quench endogenous peroxidase activity, and blocked with 5% BSA in PBS for 30 min at 37C. After samples were incubated overnight with primary antibody at 4C [mouse anti-HSPG, clone 7E12 (Invitrogen), previously proven to react specifically with agrin (Tátrai et al. 2006)], biotinylated secondary antibody (Dako) was applied for 30 min, signal was amplified using a Tyramide Signal Amplification biotin system kit (PerkinElmer; Waltham, MA), and detected using a DAB substrate kit (Vector Laboratories; Burlingame, CA) as chromogen. For the immunodetection of glypican-3, deparaffinized and rehydrated slides were heated in citrate buffer, pH 6, at 98.5C for 30 min and blocked with 5% BSA in PBS. Mouse anti-human glypican-3 antibody, clone 1G12 (BioMosaics; Burlington, VT) was applied in a dilution of 1:100 at 4C overnight. The signal was amplified by using biotinylated secondary antibody and an EnVision system (Dako) and visualized with DAB substrate. Primary antibodies were replaced by non-immune serum on negative control slides (results not shown).

Quantitative RT-PCR

For the comparison of gene expression levels, human samples were divided into three groups: (1) HCC tumor tissues (n=21), (2) non-malignant liver tissues with increased fibrogenesis, i.e., fibrosis, cirrhosis, and FNH (n=11), and (3) non-fibrotic peritumoral and healthy liver tissues (n=16). Total RNA from the tissues was isolated with TRIzol (Invitrogen) and reverse transcribed with SuperScript (Invitrogen). Relative quantification was performed using inventoried TaqMan assays for the target genes, with eukaryotic 18S rRNA as endogenous control (Applied Biosystems; Foster City, CA) on an ABI 7000 sequence detection system (Applied Biosystems). Expression values of target genes were calculated using the $2^{-\Delta Ct}$ method. Median fold

expression changes in the fibrotic and HCC sample groups were calculated relative to the median of the normal group, composed of both healthy and non-fibrotic peritumoral samples. Groups were compared by means of the Mann-Whitney U test.

Extraction and Disaccharide Analysis of Liver HS

Human liver HS was prepared from seven HCC tissues, seven non-fibrotic peritumoral liver tissues, and one healthy liver tissue. Tissues were pulverized under liquid nitrogen and defatted by suspension and agitation in acetone. Defatted tissues were air dried, homogenized in 0.1 mol/liter Tris-HCl, pH 7.9, and digested with Pronase E (Sigma-Aldrich). After tissues underwent heat denaturation and centrifugation, GAGs were recovered from the supernatant by application of a DEAE-Sephacel (aqueous ethanol suspension) anion-exchange chromatography column. After extensive washing with 0.25 mol/liter NaCl, 10 mmol/liter phosphate, pH 7.4, bound GAGs were step-eluted with 1.5 mol/liter NaCl, 10 mmol/liter phosphate, pH 7.4, and then desalted with a PD-10 column (Amersham Biosciences; Chalfont St. Giles, UK), eluted with distilled water, and finally freeze-dried. HS was digested to disaccharides by using a combination of heparinase enzymes, derivatized with aminoacridone and then separated by reverse-phase HPLC with direct fluorometric detection, to yield the disaccharide composition, as described by Deakin and Lyon (2008).

Results

Accumulation and Altered Localization of HS in Human Chronic Liver Disease

Various HS structural motifs were detected in healthy and diseased human liver samples, using the phage display-derived recombinant antibodies AO4B08, EV3C3, HS4C3, HS4E4, and RB4Ea12 (for the specificity of the antibodies, see Table 1). Representative fluorescence photomicrographs of immunoreactions are shown in Figure 1. In the lobules of the normal liver tissue (Figure 1, row A), sinusoidal walls were labeled by all antibodies, with an approximate intensity rank HS4C3 > AO4B08 ≈ HS4E4 > RB4Ea12 ≈ EV3C3. The non-sinusoidal membrane domains of hepatocytes were only faintly labeled or not labeled. In cirrhosis and FNH tissues (Figure 1, rows B and C, respectively), besides an overall increase in staining intensities, motifs specifically recognized by the AO4B08 and RB4Ea12 antibodies gained more relative importance. Unlike hepatocytes in the normal liver, liver cells in cirrhosis and FNH tissues also exhibited HS-related labeling (especially with AO4B08, HS4C3, and RB4Ea12) on their non-sinusoidal lateral surfaces as well. In HCC tissues, tumor cells showed robust membrane positivity, while intense staining seen in the tumoral stroma was largely attributable to the walls of neovessels (Figure 1, row D). The overall reaction strength was also increased compared with that of the cirrhosis and FNH tissues, and the intensity of RB4Ea12 staining became comparable with that of HS4C3 and AO4B08.

Blood vessels and bile ducts, as nonparenchymal structures, were also investigated. Blood vessel walls (Figure 1, row E) were labeled by all antibodies except RB4Ea12. The basement membranes of biliary epithelia were positively stained by AO4B08, EV3C3, and HS4E4 but not by HS4C3 and RB4Ea12 (Figure 1, row F), although results with HS4C3 showed some variability.

Accumulation of HS in the Rat Liver Fibrogenesis/Carcinogenesis Model

Liver specimens from healthy rats, as well as from animals with liver cirrhosis and multifocal HCC induced by simultaneous fibrogenic/carcinogenic treatment, were investigated with the same set of antibodies as described above. Figure 2 shows representative fluorescence photomicrographs of normal rat liver (Fig. 2, left column), cirrhotic liver with multiple HCC (middle column), as well as nonparenchymal structures (Fig. 2, right column). While the results were, in general, similar to those obtained with the human liver, a few specific differences were noted. The overall intensity rank of immunoreactions was as follows: HS4C3 ≈ AO4B08 ≈ HS4E4 > EV3C3 > RB4Ea12, which indicates that HS4E4 reacted more and RB4Ea12 less intensely to the rat samples. The sinusoidal pattern of immunolabeling in the normal and the cirrhotic liver and the microvascular pattern in HCC were analogous to those of the corresponding human structures, with the addition that a portal-to-central gradient in the intensity of sinusoidal anti-HS labeling was conspicuous in the normal rat liver lobules. In contrast with human samples, where HS staining was intensified overall in tissues with fibrogenic diseases, anti-HS labeling was increased only in HCC nodules but not in cirrhotic pseudolobules in treated rat livers. Another striking difference between human and rat diseased liver was the lack, or scarcity, of lateral plasma membrane staining of hepatocytes in the animal model. Even in areas of HCC with strong microvascular HS immunostaining, only faint or no plasma membrane labeling of tumor cells was detected. Membrane staining was also absent from biliary epithelial cells.

Results with nonparenchymal structures were similar to those obtained from the correspoding human structures. The lack of HS4C3 labeling on bile duct basement membranes was a consistent finding here. The high affinity of HS4E4 for rat tissue was evident in blood vessel walls where it brightly highlighted the smooth muscle layer of small arteries.

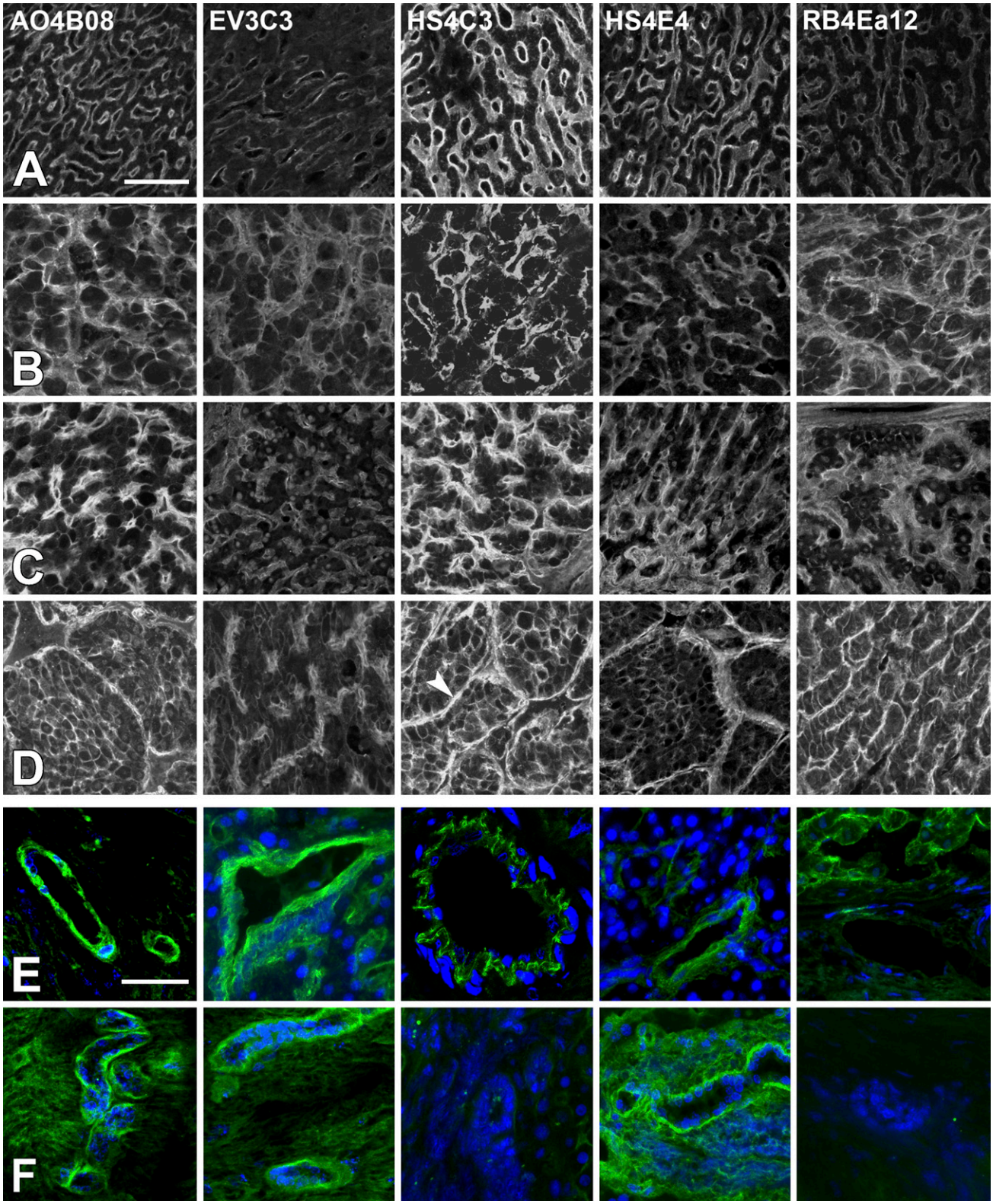

Figure 1 Immunoreactions of sulfation-specific anti–heparan sulfate (HS) antibodies in the normal and diseased human liver. Rows **A–D**, liver parenchyma; rows **E,F**: nonparenchymal structures. (**A**) normal liver tissue; (**B**) cirrhotic liver; (**C**) focal nodular hyperplasia; (**D**) hepatocellular carcinoma; (**E**) blood vessels; (**F**) bile ducts. Arrowhead in **D**, HS4C3 indicates a blood vessel belonging to the tumoral stroma. Bars: **A–D** = 100 μm; **E,F** = 50 μm.

The Journal of Histochemistry & Cytochemistry

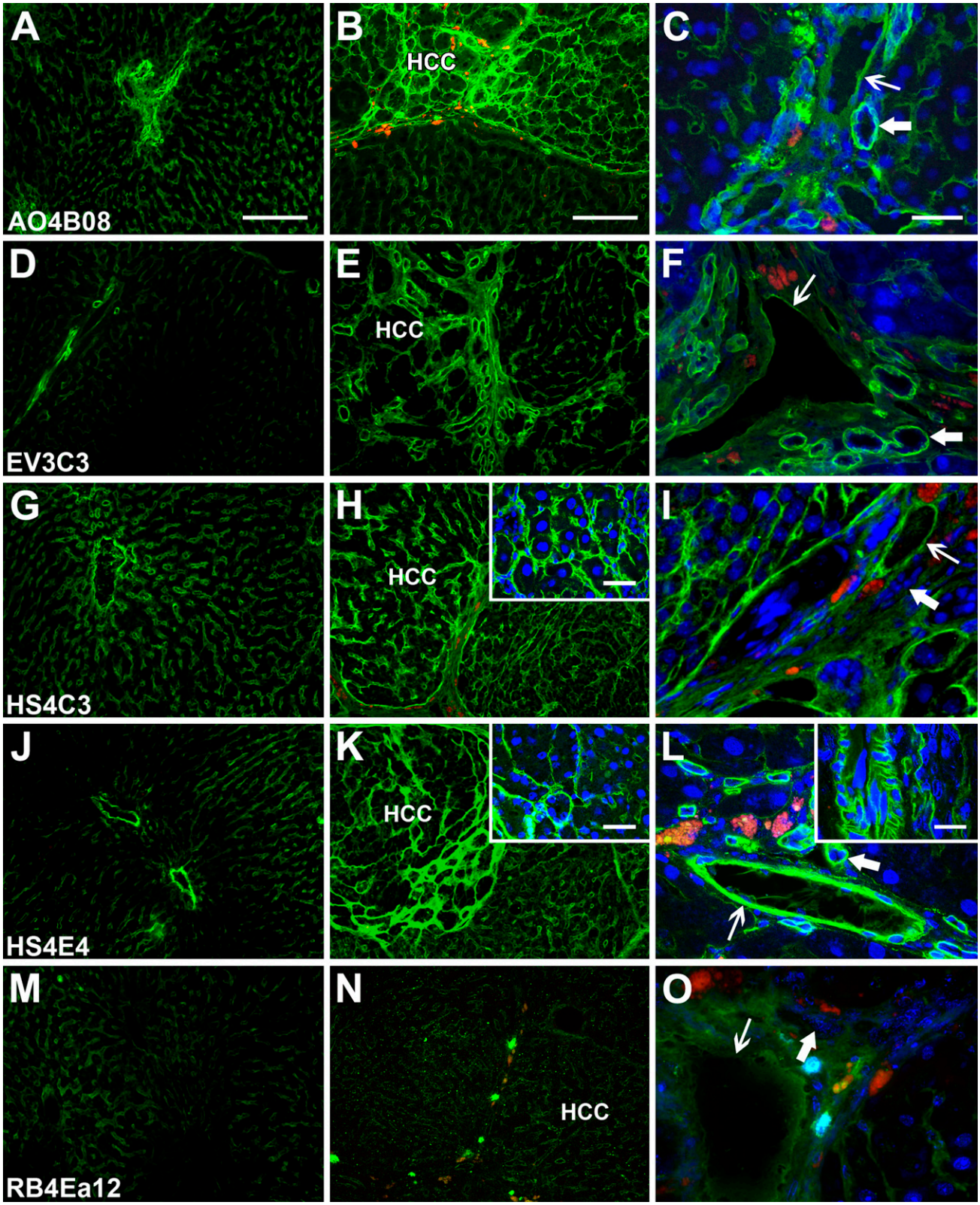

Figure 2 Immunoreactions of sulfation-specific anti-HS antibodies in normal and diseased rat liver. Left column shows healthy liver (**A,D,G,J,M**); middle column shows cirrhosis with hepatocellular carcinoma (HCC) nodules (**B,E,H,K,N**); right column shows nonparenchymal structures (**C,F,I,L,O**). Thin arrows, blood vessels; thick arrows, bile ducts. Bars: **A,B** = 250 μm (left and middle column main panels); **C** = 50 μm (right column main panels); **H,K,L** insets = 50 μm.

Accumulation and Altered Localization of Four Major HSPGs in Human Chronic Liver Disease

Syndecan-1, perlecan, agrin, and glypican-3, the four prominent HSPGs of the human liver, were detected by double-immunofluorescence (syndecan-1 and perlecan samples are shown in Figures 3A–3I) or by immunohistochemistry (as shown for agrin, glypican-3 in Figures 3J–3O). In accordance with the localization of HS, syndecan-1 and perlecan showed a predominantly sinusoidal immunostaining pattern in the healthy liver tissues (non-parenchymal structures are not shown in the figures). Sinusoidal staining for both syndecan-1 and perlecan were intensified in cirrhotic tissues; additionally, the localization of syndecan-1 extended to the entire hepatocyte membrane surface, and perlecan accumulated in association with blood vessels and bile duct basement membranes in the connective tissue septa. Syndecan-1 was also expressed on the surface of biliary epithelial cells. Glypican-3, a highly sensitive and specific marker of HCC (Wang et al. 2008), was virtually absent from the normal and cirrhotic liver. Agrin, too, was absent from the normal and cirrhotic parenchyma; however, along with perlecan, agrin appeared in blood vessel walls and bile duct basement membranes. In HCC tissue, syndecan-1 membrane labeling of tumor cells became even more intense, while the neovessels of the tumor were strongly positive for perlecan. Agrin, similar to perlecan, was localized to the microvasculature of HCC tissue. Glypican-3 exhibited a combined cell membrane and cytoplasmic staining pattern in HCC tumor cells.

Modest 6-*O*-undersulfation of HS in Human HCC

HS preparations from seven HCC tissues, seven non-fibrotic peritumoral livers, and one healthy liver were subjected to disaccharide analysis. Due to the sensitivity of the fluorescence detection and its compatibility with the presence of other biomolecules, including other GAGs, a minimal extraction and purification schedule was used to obtain GAGs from liver tissue. This schedule was also designed to minimize the opportunity for any possible postextraction modifications to the integrity and sulfation patterns of the HS due to endogenous enzyme activities (i.e, Sulfs and HPSE). Table 2 summarizes a comparison of disaccharide compositions obtained in this study with those in literature data for healthy human, rat, mouse, and porcine liver HS (Toida et al. 1997; Vongchan et al. 2005; Warda et al. 2006; Deakin and Lyon 2008). In our analyses, a markedly lower overall sulfation, primarily due to a relatively low content of trisulfated disaccharide, was observed in all the samples when compared with previously published analyses of healthy liver HS of human and other species. We observed that healthy normal liver HS and non-fibrotic, peritumoral HS were very similar in composition, while HCC samples differed slightly. Although no significant differences in the overall sulfation were seen, 6-*O*-sulfation was modestly but significantly decreased in HCC (18.0 vs 22.7 per 100 disaccharides, $p=0.002$, for HCC vs peritumoral), leading to a slight total *O*-undersulfation of tumoral HS (33.5 vs 36.7, $p=0.048$, respectively).

Quantitation of the HS extracted from the different liver samples revealed a normal liver HS content of ~107 μg/g (wet tissue weight), which compares favorably with a previously published report (80 μg/g) (Vongchan et al. 2005). However, the HS content was increased by ~50% in non-fibrotic peritumoral liver (145 ± 43 μg/g) and by >100% in HCC liver (259 ± 127 μg/g). The quantitative difference between HCC and peritumoral liver HS is weakly significant ($p=0.044$).

Increased Expression of HS Synthesis/Modification Enzymes in Human Chronic Liver Disease

mRNA expression levels of the nine enzymes (HPSE, 2-OST-1, 3-OST-1, 3-OST-3B, 6-OST-1, NDST-1 and -2, Sulf1 and -2) were investigated in the non-fibrotic ($n=16$), fibrotic ($n=11$), and HCC ($n=21$) tissue groups. Results in arbitrary expression units ($2^{-\Delta Ct} \times 10^6$) are presented in Figures 4A and 4B. Median fold expression differences of the fibrotic and HCC groups relative to the median of the non-fibrotic group are shown in Figure 4C.

Expressions of the three isozyme pairs, i.e., 3-OST-1 vs 3-OST-3B, NDST-1 vs NDST-2, and Sulf1 vs Sulf2, are compared in Figure 4A. At the mRNA level, 3-OST-3B, NDST-1, and Sulf2 were the more abundant isoforms in both the healthy and the diseased livers. Of these major isoforms, NDST-1 was modestly but significantly upregulated in both fibrosis and HCC (2.0- and 2.6-fold, respectively), while Sulf2 was significantly overexpressed (2.8-fold) in the fibrotic group only. The corresponding isozymes with lower basal expressions seemed to respond more dramatically to pathologic changes, with all three being significantly upregulated in both the fibrotic and the HCC groups. Among these, 3-OST-1 (6.4- and 7.2-fold, respectively) and Sulf1 (6.1- and 5.1-fold, respectively) were the most overexpressed of all nine investigated enzymes in the fibrotic and HCC groups, respectively, while NDST-2 (2.5- and 2.2-fold, respectively) was only moderately upregulated.

Figure 4B shows the expression levels of enzymes for which just a single isoform exists (2-OST and HPSE) or was investigated (6-OST-1). The mRNA expression levels of both 2-OST-1 and 6-OST-1 were comparable in strength to the highly expressed 3-OST and NDST isoforms, and they, too, exhibited relatively

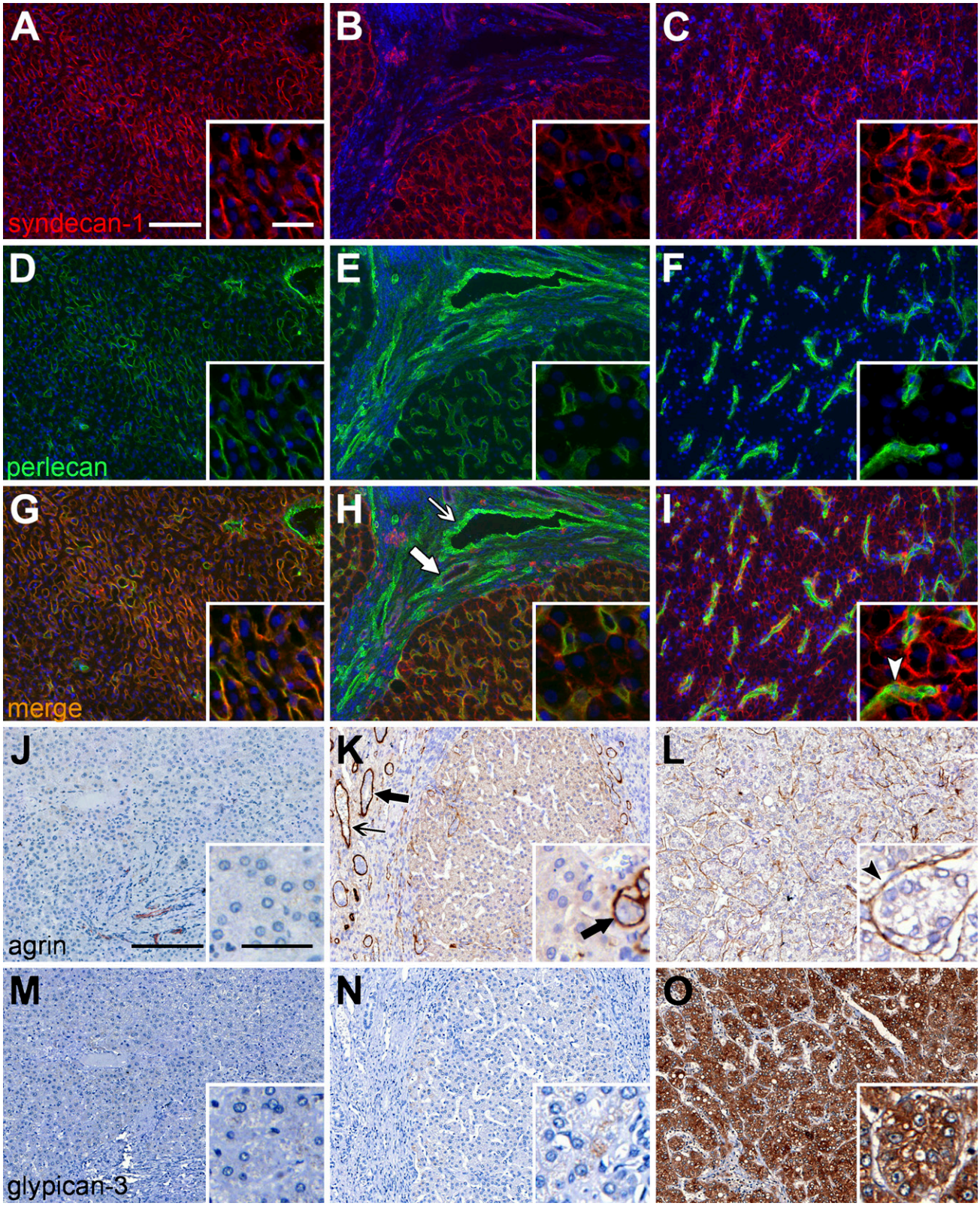

Figure 3 Immunoreactions for syndecan-1 (**A–C**), perlecan (**D–F**), agrin (**J–L**), and glypican-3 (**M–O**) in normal and diseased human liver. **G–I** show merged images of **A–C** and **D–F**. Left column shows normal liver tissue; middle column shows cirrhotic tissue; and right column shows HCC tissue. Thin arrows, blood vessels; thick arrows, bile ducts; arrowheads, HCC microvessels. Bars: **A–O** = 200 μm; insets = 50 μm. Bar in **A** applies to **A–I**; bar in **J** applies to **J–O**.

Table 2 Comparison of disaccharide analyses of diseased vs healthy tissue

	Human			Human		Rat	Mouse	Porcine
Disaccharide	HCC ± SD (n=7)	Non-fibrotic peritumoral liver ± SD (n=7)	Healthy liver ± SD (n=1)	Healthy liver[a]	HepG2 HCC cell line[b]	Healthy liver[c]	Healthy liver (male)[d]	Healthy liver[e]
ΔHexA-GlcNAc	50.4 ± 2.2	48.9 ± 0.9	49.2	37.3	46.1	31.4	50.9	47.9
ΔHexA-GlcNS	22.5 ± 1.2	20.6 ± 1.2	19.8	15.5	22.9	18.0	10.2	10.8
ΔHexA-GlcNAc(6S)	7.8 ± 1.5	11.6 ± 1.2	11.4	9.8	9.9	6.2	12.4	10.2
ΔHexA(2S)-GlcNAc	1.1 ± 0.4	1.2 ± 0.4	2.3	1.2	2.9	1.2	ND	0
ΔHexA-GlcNS(6S)	3.6 ± 0.8	4.8 ± 0.6	4.6	7.8	6.5	7.1	5.1	5.6
ΔHexA(2S)-GlcNS	7.8 ± 1.2	6.4 ± 0.9	6.1	5.9	4.4	14.4	4.4	4.4
ΔHexA(2S)-GlcNAc(6S)	ND	ND	ND	0.7	0.6	0.5	<0.5	0.0
ΔHexA(2S)-GlcNS(6S)	6.5 ± 1.2	6.2 ± 0.6	6.6	21.8	6.7	21.2	17.0	21.2
Sulfate								
N-sulfates	40.5 ± 2.2	38.2 ± 2	37.1	51.0	40.5	60.7	36.7	42.0
2-*O*-sulfates	15.4 ± 1.8	13.9 ± 1.1	15.1	29.6	14.6	37.3	21.4	25.6
6-*O*-sulfates	18.0 ± 2.9**	22.7 ± 1.1**	22.6	40.1	23.7	35.0	34.5	37.0
Total *O*-sulfates	33.5 ± 3.7*	36.7 ± 0.7*	37.7	69.7	38.3	72.3	55.9	62.6
Total sulfates	74.0 ± 5.2	75.0 ± 2.1	74.8	120.7	78.8	133.0	92.6	104.6

[a]Data from Vongchan et al. (2005).
[b]Data from Barth et al. (2003).
[c]Data from Deakin and Lyon (2008).
[d]Data from Warda et al. (2006).
[e]Data from Toida et al. (1997).
*Difference significant at p=0.048.
**Difference significant at p=0.002.
Disaccharide analyses of HS from peritumoral non-fibrotic liver tissue and hepatocellular carcinoma (HCC) compared with that from healthy liver of human, rat, mouse, and porcine origin. ΔHexA corresponds to the 4,5-unsaturated uronate residue, of either glucuronate or iduronate origin, that is generated by the lyase action of the heparinases. SD, standard deviation; ND, not determined.

small changes in disease states (2-OST-1 showed non-significant increases; and 6-OST-1 showed significant 1.8- and 2.4-fold increases in the fibrotic and HCC groups respectively). HPSE was strongly (6.1-fold) overexpressed in the fibrotic group but only by 2.0-fold in HCC.

Discussion

In the present work, by comparing normal human liver samples with samples from pathologic conditions involving increased fibrogenesis (fibrosis, cirrhosis, and FNH) and with HCC samples, we have revealed increased abundance and altered immunolocalization of various HS motifs, a modest 6-*O*-undersulfation of HS in HCC, as well as significant elevations in the mRNA levels of selected HS-modifying enzymes in the diseased liver. We found that accumulation of HS also occurs in a rat cirrhosis/HCC model. To the best of our knowledge, this is the first study to apply sulfation pattern-specific anti-HS phage display antibodies to the study of pathologic liver samples and also to compare the sulfation levels of HS from normal liver and HCC by disaccharide analysis.

In the normal human and rat liver tissue, highly sulfated HS (recognized by HS4C3 and AO4B08), HS with intermediate sulfation (recognized by RB4Ea12), and lesser sulfated HS (recognized by HS4E4) were all localized to the walls of sinusoids, central veins, and portal blood vessels, as well as to the basement membrane and epithelium of bile ducts (regarding specificities of the antibodies, see ten Dam et al. 2006; Kurup et al. 2007; and Wijnhoven et al. 2008). HS labeling of non-sinusoidal surfaces of hepatocytes was very faint or undetectable. The following inferences are based on the earlier observations of others (Roskams et al. 1995), as well as on our own previous (Kovalszky et al. 1998; Tátrai et al. 2006) and present results. Continuous sinusoidal HS labeling is thought to reflect the presence of syndecan-1 and perlecan. These HSPGs originate from the hepatocytes and sinusoidal endothelial cells. The portal-to-central intensity gradient (more readily apparent here in the rat liver but also seen in human samples) may be explained by the similar intralobular gradient observed in the expression of syndecan-1. The basolaterally accentuated HS positivity of biliary epithelial cells is probably accounted for by syndecan-1, with perlecan and agrin both being present in the bile duct basement membranes. HS positivity associated with vascular smooth muscle cells and mesenchymal cells (i.e., Ito cells, myofibroblasts) may derive from syndecan-2, syndecan-3, and perlecan. Since agrin in the healthy liver appears in the walls of portal blood vessels but not in the sinusoids, it may contribute to HS positivity in the former location only. The quantity of other HSPGs can be regarded as negligible in the healthy liver.

Surprisingly, disaccharide analysis revealed a substantially lower overall sulfation of healthy liver HS than the single previously reported study (Vongchan et al. 2005) and also than that of studies of other

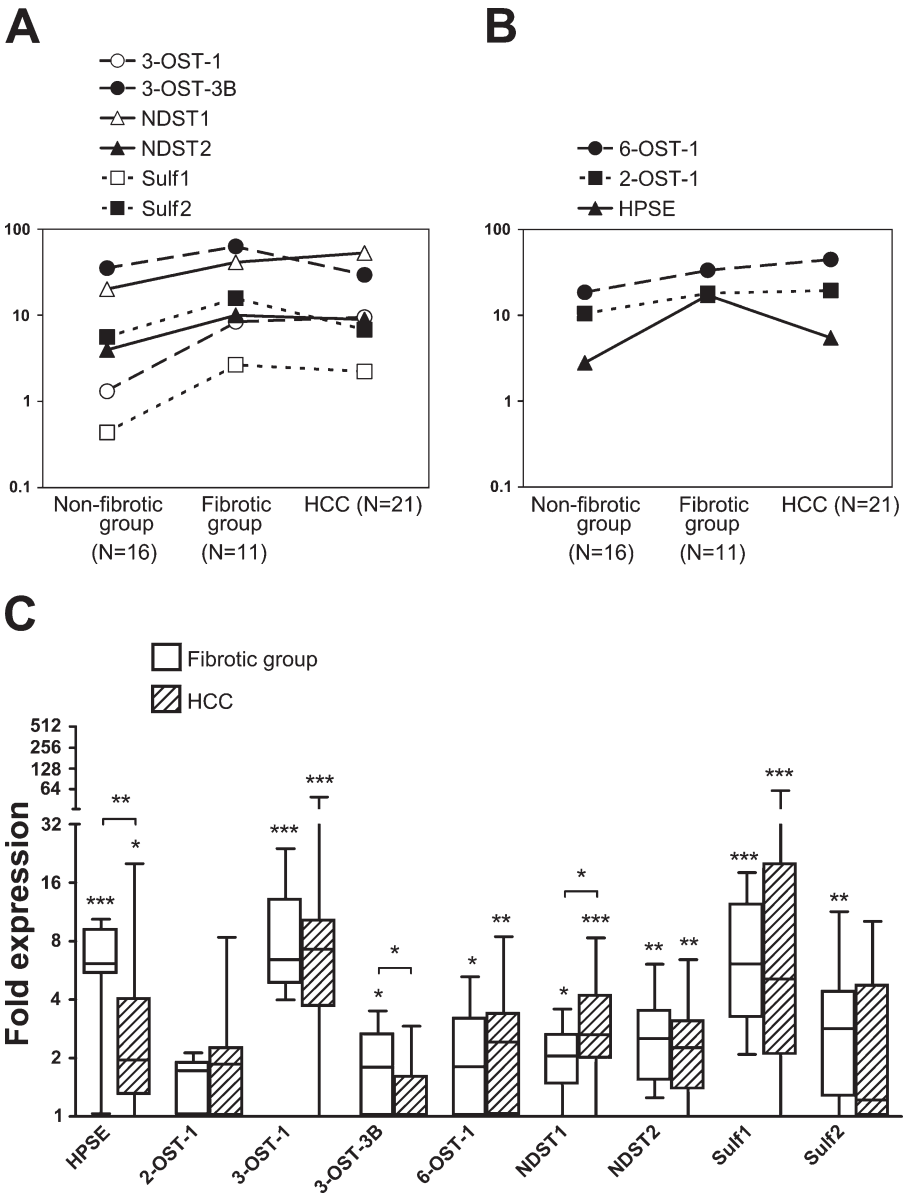

Figure 4 mRNA expression of selected HS-modifying enzymes in non-fibrotic liver, fibrogenic diseases, and HCC tissues. (**A,B**) Relative expressions of the nine enzymes in the three sample groups (reference, eukaryotic 18S rRNA) are shown in arbitrary expression units ($2^{-\Delta Ct} \times 10^6$). Isozyme pairs are compared in **A**; enzymes with only a single investigated isoform are presented in **B**. Median expression differences and minimum and maximum expression values of the nine enzymes in the fibrotic and HCC groups relative to the median of the non-fibrotic group are shown in **C**. *, $p<0.05$; **, $p<0.01$; ***, $p< 0.001$, Mann-Whitney U tests.

mammalian livers (Toida et al. 1997; Warda et al. 2006), including rat liver HS that we analyzed by using the identical method (Deakin and Lyon 2008). Bovine liver HS alone was reported to have an even lower degree of sulfation, with a complete lack of the trisulfated disaccharide motif (Hernaiz et al. 2002). The lower sulfation, in our case, is unlikely to be due to enzymatic/chemical loss of sulfates after tissue disruption and during HS extraction and purification, as we deliberately tailored the procedure to involve as few steps as possible, avoiding relatively mild conditions in which endogenous enzymes could be potentially active. We also did not use high pH alkaline elimination to remove any residual HS-linked peptide. Interestingly, the overall lower sulfation was evident at all ring positions (N, C2, and C6), implying that it is not the consequence of any single specific but artifactual loss of sulfates. An explanation for the difference with the previously published analysis remains a mystery at present. However, the composition of the normal liver HS, in the present study, is very closely mirrored by that of the HS from various samples of peritumoral liver that were near-normal histologically. Interestingly, our results generally closely resemble the composition of HS expressed by the human HCC cell line HepG2 (Barth et al. 2003) (Table 2), the only human liver cell line for which such detailed data are available.

HS-specific immunostaining, especially with AO4B08, EV3C3, and RB4Ea12 antibodies, was markedly inten-

sified in human chronic fibrogenic diseases (cirrhosis and FNH tissues). No significantly intensified HS immunostaining was seen in the non-tumorous cirrhotic liver of DPC-treated rats; it should be noted, however, that a 16-week animal model may not necessarily mirror all aspects of human liver fibrogenesis, a process typically occurring over many years or even decades. In addition to the quantitative changes, HS-related signals aberrantly appeared on the non-sinusoidal surfaces of hepatocytes in the human samples. This highly sulfated cell surface HS epitope most likely belongs to syndecan-1, given that glypican-3, another potentially membrane-bound HSPG, is not expressed in the cirrhotic liver (Zhu et al. 2001). As highly sulfated HS motifs on the hepatocyte membrane, presumably attached to syndecan-1 protein core, act as receptors for the entry of both hepatitis B and C viruses (Barth et al. 2003; Schulze et al. 2007), interference with the synthesis of syndecan-1 and/or the highly sulfated motif may be an exciting novel approach in the treatment of chronic hepatitis.

Accumulation of HS in the cirrhotic liver was accompanied by an overall boost in the enzymatic machinery of HS modification. Simultaneous upregulation of oppositely- acting enzymes such as 6-*O*-sulfotransferases and 6-*O*-sulfatases (i.e., Sulfs), as well as HPSE, indicated enhanced HS turnover. Overexpression of 3-OST-1, the most potent 3-OST isoenzyme in the generation of antithrombin III-binding sites in HS (Hernaiz et al. 2000; Girardin et al. 2005), coupled with the overexpression of HPSE that liberates anticoagulant HS and releases it into the circulation may, along with many other factors, contribute to the coagulopathy encountered in cirrhotic patients. In line with this hypothesis, a buildup of circulating anticoagulant HS was reported in a cirrhotic patient with HCC (Wages et al. 1998).

Immunostaining with all five of the epitope-specific HS antibodies was further intensified in human HCC; also, enhanced HS immunostaining, with the exception of the antibody RB4Ea12, was observed in the HCC foci of the DPC-treated rats. This may reflect the marked increase in HS present within HCC liver. Whereas HS-related immunolabeling was dominantly stromal in the rat tumors, it was associated with both the stroma and the tumor cell surfaces in human HCC. Plasma membrane HS in HCC may be contributed by both syndecan-1 and glypican-3. Although the latter often appears aberrantly in the cytoplasm of HCC cells, we saw no HS-related signals there. It is conceivable that the abnormally localized glypican-3 fails to undergo proper processing and therefore lacks recognizable HS epitopes. Stromal HS may equally belong to agrin, perlecan, and mesenchymal-type syndecans. Why cell surface HS in rats was virtually invisible to the anti-HS antibodies applied is an intriguing question that requires further investigation.

Despite the abundance of highly sulfated HS epitopes in the HCC samples, disaccharide analysis, a more sensitive and precisely quantitative method, revealed only a slight reduction in overall HS sulfation in HCC, primarily a result of a modest 6-*O*-undersulfation of HS in 5/7 samples. At the same time, the 6-*O*-endosulfatase Sulf1 was found to be more than 2-fold overexpressed in 17/21 HCCs. Others have reported that Sulf1 becomes downregulated in the majority of HCC cell lines while, in accordance with our findings, it is upregulated in nearly two thirds of human HCCs (Lai et al. 2004,2008b). The same authors also found the other Sulf isoenzyme, Sulf2, to be upregulated in almost all HCC cell lines and 60% of primary HCCs. Although we could not demonstrate a mean upregulation of Sulf2 in HCC, increased expression of the enzyme was measured in approximately half of the HCC samples. Thus, the small 6-*O*-undersulfation detected by disaccharide analysis might be related to an increased native activity of the Sulfs. The biological significance of this minor degree of 6-*O*-undersulfation is difficult to estimate, especially when taking into account the opposite effects of the two Sulfs on the progression of HCC. It has been shown in multiple cancer types, including HCC, that altered activity of the Sulfs, resulting in decreased HS sulfation, profoundly influences growth factor signaling and thereby the biological behavior of the tumor, e.g., Sulf2 activity upregulates the expression of glypican-3 and promotes fibroblast growth factor 2 signaling in HCC (Lai et al. 2008a). However, since both Sulfs were overexpressed in non-malignant fibrogenic diseases as well, a direct link between increased Sulf activity and hepatocarcinogenesis is not clear.

Finally, an important observation is the relatively high expression of a 3-*O*-sulfated HS epitope in the normal liver that further increases with disease. Unfortunately this could not be confirmed by disaccharide analyses of extracted HS, as such disaccharides are known to be very difficult to excise with heparinases and also the appropriate 3-*O*-sulfated standards are not generally available. 3-*O*-sulfated HS motifs are recognized by the antibody HS4C3 that has already been reported to react with the sinusoids in rat liver (ten Dam et al. 2006). 3-*O*-sulfation, the last and rarest step in HS modification, is carried out by the 3-OST family, which currently consists of seven isoforms with distinctive substrate specificities (Girardin et al. 2005). High expression of the isoenzymes 3-OST-3A and -3B in human liver was previously detected (Shworak et al. 1999); in our study, we saw that the massive basal expression of 3-OST-3B was maintained in both fibrogenic diseases and HCC. The 3-OST-3 isoforms and the 3-OST-5 isoenzyme are known to synthesize a 3-*O*-sulfated HS motif required for the interaction of herpes simplex virus type 1 with its target

cells (Shukla et al. 1999). Given the presence of 3-*O*-sulfated HS epitopes on the liver cell membrane in both cirrhosis and HCC and the involvement of highly sulfated HS in the docking of hepatitis B and C viruses (Barth et al. 2006; Schulze et al. 2007), it would be exciting to determine whether 3-*O*-sulfation of HS influences the attachment of hepatitis viruses to hepatocytes. Earlier studies proved the necessity of *N*-sulfation but the dispensability of 2-*O*- and 6-*O*-sulfation in the HS–hepatitis C virus interaction (Barth et al. 2006); however, the impact of 3-*O*-sulfation was not investigated. Another 3-OST isoenzyme, 3-OST-1, was previously detected in marginal amounts in healthy liver (Shworak et al. 1999). We found that in contrast to 3-OST-3B, the low basal expression of 3-OST-1 is remarkably boosted in both fibrogenic diseases and HCC. 3-OST-1, the major isoenzyme in the synthesis of antithrombin III-binding HS, is produced chiefly by endothelial and renal glomerular epithelial cells (Girardin et al. 2005). Hence, an increased expression of 3-OST-1 in liver disease may reflect pathologic changes affecting the endothelium, such as capillarization of sinusoids and tumor neovascularization. What additional roles 3-*O*-sulfated HS motifs, partly synthesized by 3-OST-1, may play besides antithrombin III binding is largely unknown. 3-*O*-sulfation was demonstrated to influence Notch signaling in *Drosophila* (Kamimura et al. 2004), whereas no corresponding human data are available. Since 3-OST-1, but not 3-OST-3B, is selectively overexpressed in diseased liver, specific inhibition of this 3-OST isoform may provide insights into its potential functions in the pathogenesis of liver fibrosis and HCC.

In summary, we revealed a relatively high abundance of 3-*O*-sulfated motifs, a selective increase in the hepatocyte plasma membrane-localized HS, and intensified expression of several HS-modifying enzymes in fibrogenic liver diseases and HCC. Also, a minor 6-*O*-undersulfation of HS was detected in HCC relative to the normal liver tissue. The significance of these observations is to be investigated in the future with special regard to HS-hepatitis virus and HS-growth factor interactions. The comparability of the rodent model with human disease gives hope that pathologic changes of liver HS may be studied in an animal system.

Acknowledgments

This work was supported by grants 67925 and 75468 from the Hungarian Scientific Research Fund (OTKA).

Literature Cited

Ashikari-Hada S, Habuchi H, Kariya Y, Itoh N, Reddi AH, Kimata K (2004) Characterization of growth factor-binding structures in heparin/heparan sulfate using an octasaccharide library. J Biol Chem 279:12346–12354

Barth H, Schafer C, Adah MI, Zhang F, Linhardt RJ, Toyoda H, Kinoshita-Toyoda A, et al. (2003) Cellular binding of hepatitis C virus envelope glycoprotein E2 requires cell surface heparan sulfate. J Biol Chem 278:41003–41012

Barth H, Schnober EK, Zhang F, Linhardt RJ, Depla E, Boson B, Cosset FL, et al. (2006) Viral and cellular determinants of the hepatitis C virus envelope-heparan sulfate interaction. J Virol 80:10579–10590

Bishop JR, Schuksz M, Esko JD (2007) Heparan sulphate proteoglycans fine-tune mammalian physiology. Nature 446:1030–1037

Blackhall FH, Merry CL, Davies EJ, Jayson GC (2001) Heparan sulfate proteoglycans and cancer. Br J Cancer 85:1094–1098

Deakin JA, Lyon M (2008) A simplified and sensitive fluorescent method for disaccharide analysis of both heparan sulfate and chondroitin/dermatan sulfates from biological samples. Glycobiology 18:483–491

Dennissen MA, Jenniskens GJ, Pieffers M, Versteeg EM, Petitou M, Veerkamp JH, van Kuppevelt TH (2002) Large, tissue-regulated domain diversity of heparan sulfates demonstrated by phage display antibodies. J Biol Chem 277:10982–10986

Dudás J, Ramadori G, Knittel T, Neubauer K, Raddatz D, Egedy K, Kovalszky I (2000) Effect of heparin and liver heparan sulphate on interaction of HepG2-derived transcription factors and their cis-acting elements: altered potential of hepatocellular carcinoma heparan sulphate. Biochem J 350:245–251

Fears CY, Woods A (2006) The role of syndecans in disease and wound healing. Matrix Biol 25:443–456

Fuster MM, Esko JD (2005) The sweet and sour of cancer: glycans as novel therapeutic targets. Nat Rev Cancer 5:526–542

Girardin EP, Hajmohammadi S, Birmele B, Helisch A, Shworak NW, de Agostini AI (2005) Synthesis of anticoagulantly active heparan sulfate proteoglycans by glomerular epithelial cells involves multiple 3-O-sulfotransferase isoforms and a limiting precursor pool. J Biol Chem 280:38059–38070

Harmer NJ (2006) Insights into the role of heparan sulphate in fibroblast growth factor signalling. Biochem Soc Trans 34:442–445

Hernaiz M, Liu J, Rosenberg RD, Linhardt RJ (2000) Enzymatic modification of heparan sulfate on a biochip promotes its interaction with antithrombin III. Biochem Biophys Res Commun 276:292–297

Hernaiz MJ, Yang HO, Gunay NS, Toida T, Linhardt RJ (2002) Purification and characterization of heparan sulfate peptidoglycan from bovine liver. Carbohydr Polym 48:153–160

Iozzo RV, Zoeller JJ, Nyström A (2009) Basement membrane proteoglycans: modulators par excellence of cancer growth and angiogenesis. Mol Cells 27:503–513

Kamimura K, Rhodes JM, Ueda R, McNeely M, Shukla D, Kimata K, Spear PG, et al. (2004) Regulation of Notch signaling by Drosophila heparan sulfate 3-O sulfotransferase. J Cell Biol 166: 1069–1079

Korc M (2007) Pancreatic cancer-associated stroma production. Am J Surg 194:S84–S86

Kovalszky I, Nagy P, Szende B, Lapis K, Szalay F, Jeney A, Schaff Z (1998) Experimental and human liver fibrogenesis. Scand J Gastroenterol Suppl 228:51–55

Kurup S, Wijnhoven TJ, Jenniskens GJ, Kimata K, Habuchi H, Li JP, Lindahl U, et al. (2007) Characterization of anti-heparan sulfate phage display antibodies AO4B08 and HS4E4. J Biol Chem 282:21032–21042

Lai JP, Chien JR, Moser DR, Staub JK, Aderca I, Montoya DP, Matthews TA, et al. (2004) hSulf1 Sulfatase promotes apoptosis of hepatocellular cancer cells by decreasing heparin-binding growth factor signaling. Gastroenterology 126:231–248

Lai JP, Sandhu DS, Yu C, Han T, Moser CD, Jackson KK, Guerrero RB, et al. (2008a) Sulfatase 2 up-regulates glypican 3, promotes fibroblast growth factor signaling, and decreases survival in hepatocellular carcinoma. Hepatology 47:1211–1222

Lai JP, Thompson JR, Sandhu DS, Roberts LR (2008b) Heparin-degrading sulfatases in hepatocellular carcinoma: roles in pathogenesis and therapy targets. Future Oncol 4:803–814

Lauer ME, Hascall VC, Wang A (2007) Heparan sulfate analysis from diabetic rat glomeruli. J Biol Chem 282:843–852

Ledin J, Ringvall M, Thuveson M, Eriksson I, Wilén M, Kusche-Gullberg M, Forsberg E, et al. (2006) Enzymatically active N-deacetylase/N-sulfotransferase-2 is present in liver but does not contribute to heparan sulfate N-sulfation. J Biol Chem 281: 35727–35734

Properzi F, Lin R, Kwok J, Naidu M, van Kuppevelt TH, ten Dam GB, Camargo LM, et al. (2008) Heparan sulphate proteoglycans in glia and in the normal and injured CNS: expression of sulphotransferases and changes in sulphation. Eur J Neurosci 27:593–604

Rops AL, van den Hoven MJ, Bakker MA, Lensen JF, Wijnhoven TJ, van den Heuvel LP, van Kuppevelt TH, et al. (2007) Expression of glomerular heparan sulphate domains in murine and human lupus nephritis. Nephrol Dial Transplant 22:1891–1902

Roskams T, De Vos R, David G, Van Damme B, Desmet V (1998) Heparan sulphate proteoglycan expression in human primary liver tumours. J Pathol 185:290–297

Roskams T, Moshage H, De Vos R, Guido D, Yap P, Desmet V (1995) Heparan sulfate proteoglycan expression in normal human liver. Hepatology 21:950–958

Roskams T, Rosenbaum J, De Vos R, David G, Desmet V (1996) Heparan sulfate proteoglycan expression in chronic cholestatic human liver diseases. Hepatology 24:524–532

Schulze A, Gripon P, Urban S (2007) Hepatitis B virus infection initiates with a large surface protein-dependent binding to heparan sulfate proteoglycans. Hepatology 46:1759–1768

Shukla D, Liu J, Blaiklock P, Shworak NW, Bai X, Esko JD, Cohen GH, et al. (1999) A novel role for 3-O-sulfated heparan sulfate in herpes simplex virus 1 entry. Cell 99:13–22

Shworak NW, Liu J, Petros LM, Zhang L, Kobayashi M, Copeland NG, Jenkins NA, et al. (1999) Multiple isoforms of heparan sulfate D-glucosaminyl 3-O-sulfotransferase. Isolation, characterization, and expression of human cdnas and identification of distinct genomic loci. J Biol Chem 274:5170–5184

Tátrai P, Dudás J, Batmunkh E, Máthé M, Zalatnai A, Schaff Z, Ramadori G, et al. (2006) Agrin, a novel basement membrane component in human and rat liver, accumulates in cirrhosis and hepatocellular carcinoma. Lab Invest 86:1149–1160

ten Dam GB, Kurup S, van de Westerlo EM, Versteeg EM, Lindahl U, Spillmann D, van Kuppevelt TH (2006) 3-O-sulfated oligosaccharide structures are recognized by anti-heparan sulfate antibody HS4C3. J Biol Chem 281:4654–4662

Toida T, Yoshida H, Toyoda H, Koshiishi I, Imanari T, Hileman RE, Fromm JR, et al. (1997) Structural differences and the presence of unsubstituted amino groups in heparan sulphates from different tissues and species. Biochem J 322:499–506

Vlodavsky I, Ilan N, Naggi A, Casu B (2007) Heparanase: structure, biological functions, and inhibition by heparin-derived mimetics of heparan sulfate. Curr Pharm Des 13:2057–2073

Vongchan P, Warda M, Toyoda H, Toida T, Marks RM, Linhardt RJ (2005) Structural characterization of human liver heparan sulfate. Biochim Biophys Acta 1721:1–8

Wages DS, Staprans I, Hambleton J, Bass NM, Corash L (1998) Structural characterization and functional effects of a circulating heparan sulfate in a patient with hepatocellular carcinoma. Am J Hematol 58:285–292

Wang HL, Anatelli F, Zhai QJ, Adley B, Chuang ST, Yang XJ (2008) Glypican-3 as a useful diagnostic marker that distinguishes hepatocellular carcinoma from benign hepatocellular mass lesions. Arch Pathol Lab Med 132:1723–1728

Warda M, Toida T, Zhang F, Sun P, Munoz E, Xie J, Linhardt RJ (2006) Isolation and characterization of heparan sulfate from various murine tissues. Glycoconj J 23:555–563

Wijnhoven TJ, van de Westerlo EM, Smits NC, Lensen JF, Rops AL, van der Vlag J, Berden JH, et al. (2008) Characterization of anticoagulant heparinoids by immunoprofiling. Glycoconj J 25:177–185

Xiao Y, Kleeff J, Shi X, Büchler MW, Friess H (2003) Heparanase expression in hepatocellular carcinoma and the cirrhotic liver. Hepatol Res 26:192–198

Zalatnai A, Lapis K (1994) Simultaneous induction of liver cirrhosis and hepatocellular carcinomas in F-344 rats: establishment of a short hepatocarcinogenesis model. Exp Toxicol Pathol 46: 215–222

Zhu ZW, Friess H, Wang L, Abou-Shady M, Zimmermann A, Lander AD, Korc M, et al. (2001) Enhanced glypican-3 expression differentiates the majority of hepatocellular carcinomas from benign hepatic disorders. Gut 48:558–564

The Journal of Histochemistry & Cytochemistry